THE JOURNAL OF PHYSICAL CHEMISTRY Letters

Letter

pubs.acs.org/JPCL

Controlling Orientational Order in 1-D Assemblies of Multivalent Triangular Prisms

Kevin L. Kohlstedt,[†,‡] Monica Olvera de la Cruz,[†,‡] and George C. Schatz*,[†]

[†]Department of Chemistry and [‡]Department of Materials Science and Engineering, Northwestern University, Evanston, Illinois 60208, United States

Supporting Information

ABSTRACT: Multivalent nanostructures are becoming an increasingly important player in the self-assembly of supramolecular lattices. Understanding the role that shape plays in the coordination of the assemblies is crucial for the functional response of the material. We develop a simple design rule for the assembly of multivalent Au triangular nanoprisms into 1-D ordered arrays based on *both* the length of the valent DNA and the aspect ratio of the prism. Using MD simulations, we describe an order parameter that captures the short-range order of the assembly controlled by the design parameters. The order parameter shows that even short chains ($N = 4$) of prisms have a high degree of orientational order that transitions to no orientational order when the DNA length is similar to the prism length. Unlike isotropic polyvalent assemblies, we find that the highly oriented chains of prisms lose orientational order in discrete steps during melting as the prisms in the arrays dissociate.

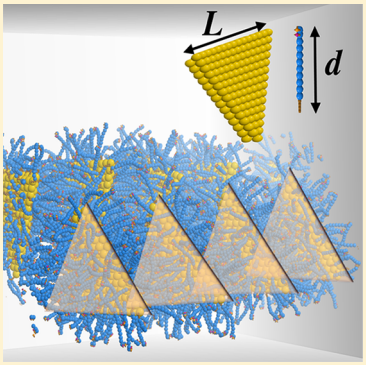

SECTION: Biophysical Chemistry and Biomolecules

The control of nanostructure valency has shown to be a key technique in controlling molecular architecture due to the exquisite control of supramolecular chemistry[1,2] and nanotechnology.[3] There exist relatively few options to dynamically control a nanostructure's valency in a precise, reversible manner,[4,5] and it has proved even more difficult to investigate the degree of order in the assembly of multivalent structures.[6] The use of of anisotropic nanostructures with coordinated directionality owing to their shape has long been sought as a method to guide assembly, but only recent synthesis techniques have allowed a wide variety of shapes and sizes to be available.[7,8] Nanoparticle assemblies comprised of anisotropic structures show novel collective behaviors including localized surface plasmon resonance, liquid-crystalline behavior, and directional superlattice assemblies.[7,9−11] These novel properties rely on assemblies of nanostructures with high-quality positional and orientational order.[12,13] There have been many purposed strategies to assemble such nanostructures,[6,14] but few offer the control and specificity of DNA-guided assembly.[15,16] A major reason is that multivalent DNA nanostructures can be derived from a sequence with exquisite sensitivity as well as from the cooperative kinetic behavior, as evidenced by the sharpened melting profile.[17]

Recently, it was reported, using DNA-guided assembly, that nanoscale Au triangular prisms can be assembled into 1-D superlattices.[12] The use of dsDNA oligomers to densely cover high aspect ratio (AR > 5) nanostructures such as triangular prisms results in particles with directionally dependent binding sites on each triangular face (see Figure 1). While the lattice parameter of the superlattice was well-characterized,[12] the orientational behavior of the prisms is not easily probed. Yet,

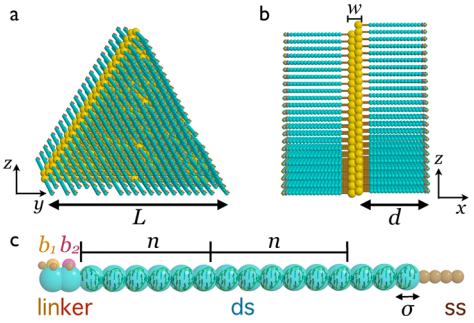

Figure 1. Model of nucleic acid and Au prism nanostructures. The prism geometry is determined by L and w, the ratio of which gives an aspect ratio (shown here as 13) (a). All prisms in this study have w = 75 Å. The DNA loading densities are taken from ref 11, and the DNA strands are placed on the (111) Au surface while allowing for random vacancies. The model nucleic acids (b) are composed of three sections, ss, ds, and linker. The ds region is composed of beads representing six base pairs and can be lengthened in units of n. Similarly, the ss beads represent three poly-A bases, while the linker region is composed of four to six bases.

functionalities such as plasmonic coupling,[8,18,19] chemical sensing,[20] and optical antennae are dependent on precise orientational control of the prisms. On the other hand, 1-D arrays are well-known not to have long-range orientational order as the entropic gain for defects increases as the array size

Received: November 26, 2012
Accepted: December 18, 2012
Published: December 18, 2012

N, which leads to correlations for only short blocks.[21] The multivalent prisms offer a unique system to examine the orientational order of a 1-D lattice due to the precise control of the aspect ratio and DNA binding distance.

In this Letter, we investigate via a coarse-grained molecular dynamic (CGMD) model the self-assembly of Au triangular nanoprisms into a 1-D superlattice. CGMD simulations allow access to mesoscales, especially important in 100−500 nm assemblies, yet they still are able to probe molecular energy and length scales such as DNA hybridization. We identify a simple design rule that describes the interplay between the prism size L and DNA length d and its effect on the coordination of the nanostructure. We describe and analyze an orientational order parameter (OP) of the assembled prisms as a function of the number of prisms N. Conversely, we show that the hybridization efficiency of the DNA linkers between the prisms alone does not effectively describe the orientational order of the assembly. Using the design rule, we describe how the prism coordination can be tuned by lengthening the dsDNA oligomers, eventually transforming the prisms into a spherically coordinated polyvalent structure, recovering previous observations for spherical nucleic acids (SNA).[15] Finally, we show the effects of melting on the orientational order of the superlattice.

We consider a coarse-grained (CG) model for thiolated 18−90 bp dsDNA on Au triangle prisms inspired from an ssDNA model by Knorowski et al.[22] and successfully implemented for the dsDNA superlattice assembly.[23] The DNA oligomer consists of three parts, an A10 ssDNA spacer that is thiolated to the Au surface (5′), a dsDNA spacer extendable in blocks of n containing 39 base pairs and 4−6 self-complementary bases acting as a sticky linker (3′). The geometry of the DNA-Au structure in the description of our model is detailed in Figure 1. The prism is uniquely described by the length L because for all prisms, the thickness is held constant at 75 Å. We keep the prism geometry fixed using rigid-body dynamics in the HOOMD-blue MD package.[24,25] We consider here three prism sizes L = 60, 96, and 140 nm that are experimentally realizable[12] but focus on L = 60 nm as bigger prisms just rescale the geometry and dynamics. Another length scale of the system is the length of the DNA oligomer d, which is controlled by the number of ds spacer blocks n. It is convenient to scale the DNA length by the length of the prism as it gives a measure of the sphericity of the structure $S = d/L$, where d is the averaged end-to-end distance of the DNA oligomers. Each oligomer is built from harmonically bonded beads with the ds beads stiffened with a harmonic angular potential V_{angle}. Force field details and parameters are tabulated in the Supporting Information. The interparticle beads interact via a repulsive soft hydration shells modeled as the WCA potential.[26] The van der Waals diameter of each type of bead is tabulated in Table 1. The linker beads b_1,b_2, which account for the attractiveness of the self-complementary terminal 4−6 bases, allow hybridization only between interprism linkers, for example, b_1 attracts b_2 and is repulsive otherwise. The choice of the linker beads uniquely selects the ΔG of hybridization (see Table 1) but does not qualitatively alter the assembly, and we present the GCGC linker for the remainder of the Letter.

Table 1. CGMD Model Parameters

linker	ΔG (kcal/mol)	σ_b (Å)	σ_{ss} (Å)	σ_{ds} (Å)
GCGC	−10.0	10	10	20
TGCGCA	−13.8	12	10	20
TGCA	−7.1	10	10	20

The Au prisms are composed of two (111) fcc faces that provide dense surface coverages (ρ = 0.031 DNA/nm^2), which allow for 3.2 nm of surface lateral movement. We used an orthorhombic simulation cell (l_x = 100−400 nm) in order to keep the Au prisms at experimental concentrations of $\rho_{\text{Au}} \approx 5$ nM. Up to 10 random trajectories were run for 1−4 μs in order to fully sample the assembly pathway and establish equilibrium configurations. For larger systems with $N > 10$, it became important to thermally anneal to allow aggregates to elongate before equilibrium was established.

To address the order of the 1-D superlattice of Au prisms, we begin by determining an appropriate order parameter that captures the orientation of the prisms in their superlattice assemblies. We start by finding the suitable conditions when a prism is correlated with its neighbors. It is important to recall that in 1-D assemblies, long-range order is destroyed by thermal fluctuations, but short-range correlations appear in many systems.[27] The anisotropic nature of the prism geometry naturally leads to expressing the position and orientation of the ith prism in terms of a face-normal $\mathbf{N}_i$ (up to inversion symmetry), face-tangent $\mathbf{T}_i$ (up rotations of $2n_r\pi/3$), and centroid position $\mathbf{r}_i$. We consider a prism to be correlated with its neighbors if the face-normal and face-tangent are aligned. This leads to the following three conditions for short-range order: (1) the face-normal $\mathbf{N}_i$ must be aligned with the lattice axial vector $\mathbf{A}_N$ of stack size N, for example, $|\mathbf{N}_i \cdot \mathbf{A}_N - 1|^2 < \varepsilon_A^2$, (2) the face-tangent $\mathbf{T}_i$ is aligned such that the vertices are commensurate, and (3) the prism distance $D_{ij} \equiv |\mathbf{r}_i - \mathbf{r}_j|$ must be close enough to allow the linkers to hybridize or $(D_{ij} - 2d)^2 < \varepsilon_d^2$. From the simulations, the small parameters based on the conditions for the B-form to hybridize, that is, a maximum rise-per-base pair of 3.4 Å/bp, are ε_A = 0.08 and $\varepsilon_d = 20n$ Å. We show the degrees-of-freedom for a prism i adding to a stack of size N, with the labeled orientations, in the lower inset of Figure 2a. Using the above criteria, we can track the formation of order in 1-D prism stacks during the simulation trajectory.

We begin by comparing the lattice constant a predicted from our model with that measured by SAXS as a function of dsDNA length in ref 12. In Figure 2a, we plot the ensemble-averaged $a \equiv \langle D_{ij} \rangle$ for n = 1−4 spacers and find excellent agreement with the SAXS lattice constants. The regression of the lattice constants gives a rise-per-base pair of 0.27 nm/bp, consistent with the 0.281 reported in ref 11 and substantially less than the Watson−Crick value. We note that this result is in agreement with atomistic MD simulations of tethered dsDNA.[28] Further, they show that the DNA does not alter its conformation from the B-form but geometrically kinks at the linker region, accounting for the smaller rise-per-base pair (they additionally show the ss A10 spacer partially adsorbed to the Au surface). We find here a bend angle Θ that is strikingly similar to what was found previously.[28,29] We show the average bend angle Θ = 146° ± 15° in Figure 2b, which compares well with that from previous studies.[28,29]

In Figure 2a, we show that the persistence length of dsDNA (l_{ds}) occurs between n = 1 and 2 near a = 58 nm (accounting for the prism thickness w). The fact that we find ordered lattices at almost $a \approx 2l_{ds}$ points to the correlating effect that surface-bound DNA has compared to free DNA. In order to track the correlation of DNA length during assembly, we also calculate the distribution of DNA lengths $p(d)$ (n = 1) for both isolated and assembled prisms, and we observe a narrowing of

dx.doi.org/10.1021/jz301953k | J. Phys. Chem. Lett. 2013, 4, 203−208

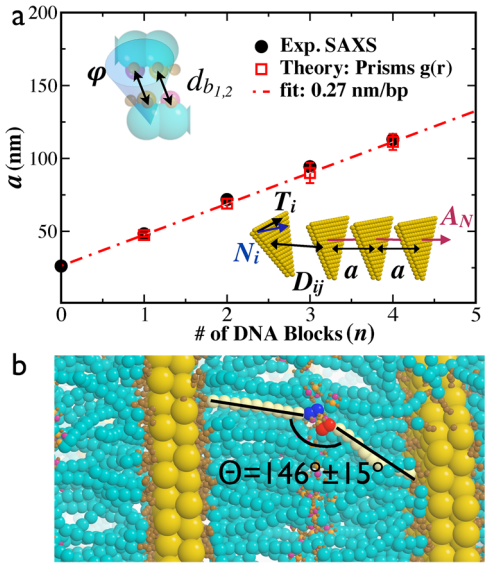

Figure 2. The prism lattice constant for a 1-D superlattice as a function of n ds-DNA blocks for prisms with L = 60 nm (a). The slope and intercept of the line connecting data points (red squares) from n = 1 to 4 match well with the SAXS data (black circles) from ref 12. For L = 60 nm, all DNA lengths considered here satisfy d/L < 1, hence keeping face valency. The upper inset shows the DNA linker hybridization geometry. The lower inset illustrates prism orientation vectors used in the OP calculation. (b) The bent conformation between two linking oligomers gives a bend angle of θ = 146°.

the lengths post assembly (see the Supporting Information). It is possible that the DNA environment may lead to an attractive force that mechanically stabilizes the bent DNA conformations.

The genesis of such a force remains somewhat of a mystery as it has been shown that the conformation of the DNA secondary structures remains in its B-form.[28] One explanation could be due to the interface of two different dielectric media. Sharp differences between bulk and DNA salt concentrations (5-fold) exist, and the dielectric response of the DNA region is lowered compared to that of the bulk aqueous solution.[30] We can write the force (per area) between the Au surfaces in the limit of small linker distances $D \ll d$ as[31]

$$F(D) = \frac{A_{\mathrm{DNA-bulk-DNA}}}{6\pi D^3} \quad (1)$$

where $D \equiv a - 2d$ and $A_{\mathrm{DNA-bulk-DNA}}$ is the interfacial Hamaker constant between the DNA and bulk dielectric regions. For symmetric interfaces, it can be shown that the Hamaker constant is definitely positive and can be approximated as $A_{\mathrm{DNA-bulk-DNA}} \approx [(A_{\mathrm{DNA}})^{1/2} - (A_{\mathrm{bulk}})^{1/2}]^2$.[31] Indeed, for mismatched dielectric constants $\varepsilon_{\mathrm{DNA}} < \varepsilon_{\mathrm{bulk}}$, salt ions at the interfaces will deplete the region due to repulsive image charges, resulting in the ions in the lower dielectric environment ($\varepsilon_{\mathrm{DNA}}$) feeling less confined.[32] This effect would tend to decrease the amount of entropic repulsion between the two DNA layers. On the other hand, the DNA strands gain free volume to rotate when bent, and the collective behavior of many DNA may account for a net entropic attraction between the prisms. We do not add an effective attractive force between the prisms in this work, but note that even with a homogeneous background dielectric, we find similar bent DNA configurations to those in ref 28.

We also track the fraction of hybridized linkers to account for the face-to-face 'binding efficiency" of the prisms. We use a two-point correlation function between (b_1,b_2) pairs. We consider a linker hybridized when *both* d_b < 18 Å and ϕ < 30°, where ϕ is the angle swept out by the base directors shown in the upper inset of Figure 2a. The bonding parameters were chosen to allow partial bonding between the pair of bases but not singlet pairing nor highly rotated base pairing. Using the above conditions, we tracked the interprism linker hybridization efficiency

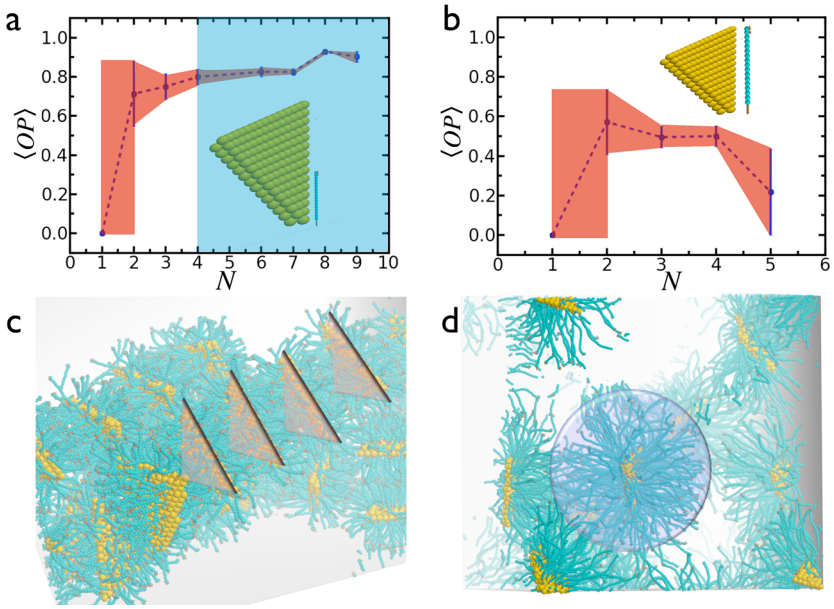

Figure 3. Prismatic design rule for nanostructure valency. The ⟨OP⟩ is plotted as a function of lattice size N for two sphericities $S \equiv d/L$ = 0.35 (n = 1) (a) and S = 1.1 (n = 5) (b). Short-range orientational order is visibly missing as $d/L \to 1$, and the 1-D superlattice is no longer assembled, while the onset of order for S = 0.35 begins at N = 4 (blue shading in a). Equilibrium structures for S = 0.35 and 1.1 show a characteristic assembly for prisms with face valency (c) and continuous valency (d), respectively.

dx.doi.org/10.1021/jz301953k | J. Phys. Chem. Lett. 2013, 4, 203−208

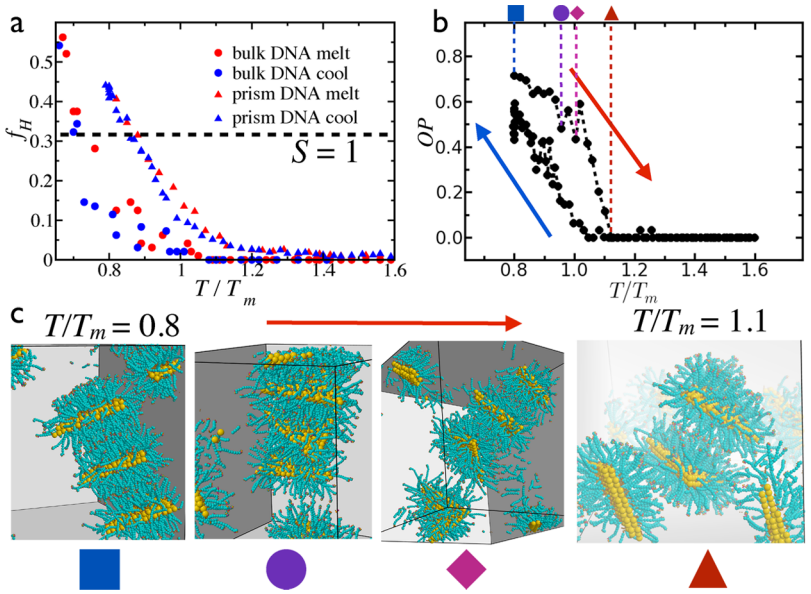

Figure 4. The interplay between the DNA multivalency and the prism anisotropy leads to a multistage melting of the superlattices. The fraction of DNA linkers hybridized f_H, for DNA between prisms (triangles) and free DNA (circles), transitions from ordered arrays to isolated prisms through T_m (a). We also show the maximum hybridization efficiency for continuously polyvalent prisms ($S > 1$) (e.g., spheres in ref 23). The OP for a four-prism superlattice shows a multistage melting trajectory, where each minima in OP is the edge melting of a prism and subsequent peaks show the remaining aggregate gaining order after the $N - 1$ prism melts (b). Each melt stage of the four-prism assembly is denoted by the square, circle, diamond, and triangle. The corresponding snapshot is shown is shown in a step-by-step fashion, where the snapshots exactly correspond to matching symbols in the OP plot (c).

$$f_H \equiv \frac{\#\text{ of hybridized linkers}}{\#\text{ of possible linker pairs}} \qquad (2)$$

as a function of time above and below the T_m of the linkers, illustrated in the Supporting Information and discussed in further detail below in the melting of the superlattices. We find that the hybridization efficiency for the prisms is ~50% greater than that predicted for SNA superlattices,[23] and it follows the findings of increased binding affinity for anisotropic structures.[11] Of course, because we do not include discrete ions in our CG model, we do not recover the cooperativity due to ion cloud sharing.[17,33]

We now consider the effects of the length of the dsDNA spacer and its effect on the sphericity S of the prisms and subsequent assembly properties. We compare the short-range orientational order between two systems $S \ll 1$ and $S \sim 1$. At $S \ll 1$, the binding valency of the linkers is highly anisotropic, leading to 1-D superlattice stacks. When the length of the DNA becomes comparable to the length of the prism or $S = 1$, the DNA binding valency becomes isotropic, and the 1-D assemblies transition to 3-D assemblies, as shown in Figure 3c,d. This transition is vividly captured with a local order orientational parameter defined as

$$\langle \mathrm{OP} \rangle = \left\langle \frac{\mathrm{mod}[\mathbf{T}_i \cdot \mathbf{T}_j,\ 2n_r\pi/3]}{N} \right\rangle \qquad n_r = 1,\ 2,\ 3 \qquad (3)$$

which measures nearest-neighbor alignment of prisms averaged over the configurational space. In Figure 3, we compare the ⟨OP⟩ for $S = 0.35$ ($n = 1$; Figure 3a) and $S = 1.1$ ($n = 5$; Figure 3b). The ⟨OP⟩ clearly captures a design rule for the coordination of the prisms governed by the two fundamental length scales of the assemblies: L and d. We describe the design rule as follows. Prismatic Design Rule: The valency coordination of the prisms is controlled by the ratio of the DNA length d and the prism length L. Continuously polyvalent nanostructures (spherical symmetry) form for $d/L \approx 1$, while $d/L < 1$ leads to a face-coordinated prism that forms aligned 1-D stacks.

In Figure 3a, we plot the per prism ⟨OP⟩ as function of the array size N (see above for conditions of local order) for up to $N = 8$ prisms. For $N < 4$, the orientation of the stacks is not well-aligned; ⟨OP⟩ < 0.8 with large rotational deviations occurring, as shown by the red shading in Figure 3a. A well-defined ordered array is shown for $N \geq 4$, where the ⟨OP⟩ plateaus and rotation fluctuations are damped. We highlight in Figure 3b an $N = 4$ aligned array among an ensemble of assembled prisms. We note that we never find perfectly ordered structures for $N \to \infty$ as long-range order is not predicted for 1-D assemblies.[21]

By comparison, the polyvalent prisms in Figure 3b,d do not form long-lived oriented stacks for $N \geq 4$. In fact, no like-oriented stacks of $N > 5$ were ever made for the entire ensemble-averaged system over 10 independent trajectories and $t \approx 5$ μs. Interestingly, only dimers of prisms ($N = 2$) had weak orientational correlations ⟨OP⟩ > 0.5, which quickly decayed to randomly oriented arrangements by $N = 5$. The lack of orientational alignment further corresponds to a lack in positional and face-normal correlation, as shown in Figure 3d, where disordered 3-D assemblies are shown. In the large-N limit, we expect a transition to a fcc phase.[11,23]

The orientational order parameter during the melting of 1-D assemblies provides additional valuable insight into the loss of order for increasing T. We examine here the hybridization profile during a slow temperature ramp of $\Delta T/\Delta t = 2.2$ °C ns^{-1}. We chose a prism array with $N = 4$ prisms to minimize self-interactions yet still be highly orientationally ordered. Figure 4a shows the fraction of DNA linkers hybridized as a function of temperature T. While we are not able to recover the sharp melting due to the salt cloud cooperativity,[17,33] we find

dx.doi.org/10.1021/jz301953k | J. Phys. Chem. Lett. 2013, 4, 203−208

that there is some steric cooperativity compared to free DNA (see Figure 4a). We also find inhibitive cooperation and binding dynamism as only nearly half of the DNA linkers are hybridized at any given time for the lowest T considered, yet it is nearly 50% more than that predicted for spherical DNA assemblies.[23] We expect that during the melting of anisotropic nanostructures, the loss in order should be qualitatively different from close-packed cubic superlattices,[34] which is not captured in f_H due to the dynamic nature of forming and re-forming bonds. Instead, we focus on the rotational alignment of the Au prisms during the melting process. We again employ the orientation order parameter of the aggregate, but instead of calculating an ensemble-averaged $\langle OP \rangle$, we calculate an instantaneous OP at each T for the $N = 4$ aggregate. In Figure 4b, we immediately notice a stair-step feature in the OP that is not captured in f_H. To understand the stair-step feature, we examine the $N = 4$ structure at the base of each step denoted by the filled square, circle, diamond, and triangle symbols in Figure 4b, with the matching structure in Figure 4c. It is evident from the sequence of structures that at each step, the rotational order of the aggregate is disturbed until a prism detaches, allowing the remaining $N - 1$ aggregate to "step up" in orientational order. This proceeds in step-like fashion for N, $N - 1$, $N - 2$, ... until the dimer ($N = 2$) is melted and all prisms are orientationally uncorrelated or OP = 0. For completeness, we show the full temperature cycle in both Figure 4a,b with an inverse cooling ramp. Figure 4b shows significant hysteresis but not the same stair-step aggregation due to preliminary assembly configurations that are not commensurate with the 1-D stack. We expect the multistage melting to be important during annealing cycles that grow the array sizes as only short blocks of $N \approx 10$ have been grown.[12] The OP in Figure 4b shows that the loss of orientational order at the terminal ends of the array may inhibit the $N + 1$ prism joining the array.

In summary, we derive a simple design rule that controls the assembly of DNA-guided Au nanostructures and the resultant orientational order. Using our CGMD model, we predict a structure of the prisms in a 1-D assembled superlattice that compares very well to previous experimental measurements.[11] We show that the loss of face-to-face coordination of the prisms is determined when the ratio of two principal length scales (the edge length of the prism L and the end-to-end distance of the surface DNA d) is unity. The transition between ordered and disordered prisms is vividly seen through a short-range orientational order parameter, which captures the increase in order for finite length assemblies for short DNA, and conversely, the lack of 1-D order occurs in the limit of $S \rightarrow 1$. This approach shows that multivalent nanostructures can transition between 1-D and 3-D coordination via the loss of directional binding. Slow melting of the assemblies further illustrates that the loss in short-range order occurs in the alignment of the prism vertices, leading to a stair-step loss in the orientational order of the superlattice. We expect this multistage melting behavior to be competitive with salt-induced cooperativity in DNA melting as well as polydispersity in the prism geometry. The inclusion of a simple Primitive model treatment of electrostatics within the CG model should elucidate the interplay between DNA melting and shape.

The complex behavior of the shape in nanostructure assemblies allows for novel applications especially in the area of plasmon coupling.[7] Simple design rules for lattice structures are key toward developing a framework between nanostructure shape and the coordination of the assembly.[15] Given the increasing complexity in the possible shapes of nanostructures and the specificity of DNA oligomers, we expect that design rules will become key in predicting the properties of the assembled structures.

■ ASSOCIATED CONTENT

Supporting Information

Description of simulation details, DNA hybridization efficiency, and prism pair correlation function. This material is available free of charge via the Internet at http://pubs.acs.org.

■ AUTHOR INFORMATION

Corresponding Author

*E-mail: schatz@northwestern.edu.

Notes

The authors declare no competing financial interest.

■ ACKNOWLEDGMENTS

This work was supported by AFOSR MURI Grant FA9550-11-1- 0275 at the International Institute for Nanotechnology at Northwestern University and the NSF Grant CHE-1147335. K.L.K. thanks Ting Li for early discussions of the CGMD model and Matt Jones for sharing the experimental work on the prism superlattice assembly. The authors acknowledge One-Sun Lee and Jos Zwanikken for their careful comments and helpful discussions.

■ REFERENCES

(1) Rybtchinski, B. Adaptive Supramolecular Nanomaterials Based on Strong Noncovalent Interactions. *ACS Nano* **2011**, *5*, 6791−6818.

(2) Badjic, J. D.; Nelson, A.; Cantrill, S. J.; Turnbull, W. B.; Stoddart, J. F. Multivalency and Cooperativity in Supramolecular Chemistry. *Acc. Chem. Res.* **2005**, *38*, 723−732.

(3) Palmer, L. C.; Stupp, S. I. Molecular Self-Assembly into One-Dimensional Nanostructures. *Acc. Chem. Res.* **2008**, *41*, 1674−1684.

(4) Pieters, G.; Pezzato, C.; Prins, L. J. Reversible Control over the Valency of a Nanoparticle-Based Supramolecular System. *J. Am. Chem. Soc.* **2012**, *134*, 15289−92.

(5) Gestwicki, J. E.; Cairo, C. W.; Strong, L. E.; Oetjen, K. A.; Kiessling, L. L. Influencing Receptor−Ligand Binding Mechanisms with Multivalent Ligand Architecture. *J. Am. Chem. Soc.* **2002**, *124*, 14922−14933.

(6) Young, K. L.; Jones, M. R.; Zhang, J.; Macfarlane, R. J.; Esquivel-Sirvent, R.; Nap, R. J.; Wu, J. S.; Schatz, G. C.; Lee, B.; Mirkin, C. A. Assembly of Reconfigurable One-Dimensional Colloidal Superlattices Due to a Synergy of Fundamental Nanoscale Forces. *Proc. Natl. Acad. Sci. U.S.A.* **2012**, *109*, 2240−2245.

(7) Jin, R. C.; Cao, Y. C.; Hao, E. C.; Metraux, G. S.; Schatz, G. C.; Mirkin, C. A. Controlling Anisotropic Nanoparticle Growth Through Plasmon Excitation. *Nature* **2003**, *425*, 487−490.

(8) Zhang, J.; Li, S. Z.; Wu, J. S.; Schatz, G. C.; Mirkin, C. A. Plasmon-Mediated Synthesis of Silver Triangular Bipyramids. *Angew. Chem., Int. Ed.* **2009**, *48*, 7787−7791.

(9) Patti, A.; El Masri, D.; van Roij, R.; Dijkstra, M. Collective Diffusion of Colloidal Hard Rods in Smectic Liquid Crystals: Effect of Particle Anisotropy. *J. Chem. Phys.* **2010**, *132*, 224907.

(10) Park, H. G.; Joo, J. H.; Kim, H. G.; Lee, J. S. Shape-Dependent Reversible Assembly Properties of Polyvalent DNA−Silver Nanocube Conjugates. *J. Phys. Chem. C* **2012**, *116*, 2278−2284.

(11) Jones, M. R.; Macfarlane, R. J.; Prigodich, A. E.; Patel, P. C.; Mirkin, C. A. Nanoparticle Shape Anisotropy Dictates the Collective Behavior of Surface-Bound Ligands. *J. Am. Chem. Soc.* **2011**, *133*, 18865−18869.

(12) Jones, M. R.; Macfarlane, R. J.; Lee, B.; Zhang, J. A.; Young, K. L.; Senesi, A. J.; Mirkin, C. A. DNA−Nanoparticle Superlattices

Formed from Anisotropic Building Blocks. *Nat. Mater.* **2010**, *9*, 913−917.
(13) Platt, M.; Willmott, G. R.; Lee, G. U. Resistive Pulse Sensing of Analyte-Induced Multicomponent Rod Aggregation Using Tunable Pores. *Small* **2012**, *8*, 2436−2444.
(14) Zhang, Y. G.; Lu, F.; van der Lelie, D.; Gang, O. Continuous Phase Transformation in Nanocube Assemblies. *Phys. Rev. Lett.* **2011**, *107*, 135701.
(15) Macfarlane, R. J.; Lee, B.; Jones, M. R.; Harris, N.; Schatz, G. C.; Mirkin, C. A. Nanoparticle Superlattice Engineering with DNA. *Science* **2011**, *334*, 204−208.
(16) Xiong, H. M.; van der Lelie, D.; Gang, O. Phase Behavior of Nanoparticles Assembled by DNA Linkers. *Phys. Rev. Lett.* **2009**, *102*, 015504.
(17) Jin, R. C.; Wu, G. S.; Li, Z.; Mirkin, C. A.; Schatz, G. C. What Controls the Melting Properties of DNA-Linked Gold Nanoparticle Assemblies? *J. Am. Chem. Soc.* **2003**, *125*, 1643−1654.
(18) Payne, E. K.; Shuford, K. L.; Park, S.; Schatz, G. C.; Mirkin, C. A. Multipole Plasmon Resonances in Gold Nanorods. *J. Phys. Chem. B* **2006**, *110*, 2150−2154.
(19) Hicks, E. M.; Zou, S. L.; Schatz, G. C.; Spears, K. G.; Van Duyne, R. P.; Gunnarsson, L.; Rindzevicius, T.; Kasemo, B.; Kall, M. Controlling Plasmon Line Shapes Through Diffractive Coupling in Linear Arrays of Cylindrical Nanoparticles Fabricated by Electron Beam Lithography. *Nano Lett.* **2005**, *5*, 1065−1070.
(20) Lee, K. S.; El-Sayed, M. A. Gold and Silver Nanoparticles in Sensing and Imaging: Sensitivity of Plasmon Response to Size, Shape, and Metal Composition. *J. Phys. Chem. B* **2006**, *110*, 19220−19225.
(21) Thouless, D. J. Long-Range Order in One-Dimensional Ising Systems. *Phys. Rev.* **1969**, *187*, 732.
(22) Knorowski, C.; Burleigh, S.; Travesset, A. Dynamics and Statics of DNA-Programmable Nanoparticle Self-Assembly and Crystallization. *Phys. Rev. Lett.* **2011**, *106*, 215501.
(23) Li, T. I. N. G.; Sknepnek, R.; Macfarlane, R. J.; Mirkin, C. A.; de la Cruz, M. O. Modeling the Crystallization of Spherical Nucleic Acid Nanoparticle Conjugates with Molecular Dynamics Simulations. *Nano Lett.* **2012**, *12*, 2509−2514.
(24) Nguyen, T. D.; Phillips, C. L.; Anderson, J. A.; Glotzer, S. C. Rigid Body Constraints Realized in Massively-Parallel Molecular Dynamics on Graphics Processing Units. *Comput. Phys. Commun.* **2011**, *182*, 2307−2313.
(25) Anderson, J. A.; Lorenz, C. D.; Travesset, A. General Purpose Molecular Dynamics Simulations Fully Implemented on Graphics Processing Units. *J. Comput. Phys.* **2008**, *227*, 5342−5359.
(26) Weeks, J. D.; Chandler, D.; Andersen, H. C. Role of Repulsive Forces in Determining Equilibrium Structure of Simple Liquids. *J. Chem. Phys.* **1971**, *54*, 5237.
(27) Srivastava, S.; Kotov, N. A. Nanoparticle Assembly for 1D and 2D Ordered Structures. *Soft Matter* **2009**, *5*, 1146−1156.
(28) Lee, O. S.; Cho, V. Y.; Schatz, G. C. A- to B-Form Transition in DNA Between Gold Surfaces. *J. Phys. Chem. B* **2012**, *116*, 7000−7005.
(29) Lee, O. S.; Schatz, G. C. Conformation of DNA Between Gold Surfaces. *J. Comp. Theor. Nanosci.* **2010**, *7*, 2568−2573.
(30) Zwanikken, J. W.; Guo, P. J.; Mirkin, C. A.; de la Cruz, M. O. Local Ionic Environment around Polyvalent Nucleic Acid-Functionalized Nanoparticles. *J. Phys. Chem. C* **2011**, *115*, 16368−16373.
(31) Israelachvili, J. *Intermolecular and Surcace Forces*, 2nd ed.; Academic Press: New York, 1991.
(32) Jha, P. K.; Zwanikken, J. W.; de la Cruz, M. O. Understanding Swollen-Collapsed and Re-entrant Transitions in Polyelectrolyte Nanogels by a Modified Donnan Theory. *Soft Matter* **2012**, *8*, 9519−9522.
(33) Eryazici, I.; Prytkova, T. R.; Schatz, G. C.; Nguyen, S. T. Cooperative Melting in Caged Dimers with Only Two DNA Duplexes. *J. Am. Chem. Soc.* **2010**, *132*, 17068−17070.
(34) John, B. S.; Stroock, A.; Escobedo, F. A. Cubatic Liquid-Crystalline Behavior in a System of Hard Cuboids. *J. Chem. Phys.* **2004**, *120*, 9383−9389.